AIAA JOURNAL
Vol. 43, No. 6, June 2005

Single-Cycle Performance of Idealized Liquid-Fueled Pulse Detonation Engines

S. Cheatham* and K. Kailasanath†
U.S. Naval Research Laboratory, Washington, D.C. 20375

Single-cycle performance estimates of an idealized liquid-fueled pulse detonation engine (PDE) are derived from numerical simulations of detonation of JP-10 fuel droplets in oxygen and in air. Results for a range of fuel droplet sizes, as well as results when some of the fuel is prevaporized, are discussed. For JP-10–O_2, calculations indicate that fuel-based specific impulse is comparable between different cases when the detonation is fully developed by the time it reaches the end of the detonation tube. Time-dependent thrust results, however, depend significantly on the initial form of the fuel. Degradation in total performance occurs when droplet sizes are so large that full transition to a self-propagating state cannot be reached by the end of the tube. For JP-10–air mixtures, results are similar, but stricter constraints on droplet size and prevaporization level for near-full performance exist. (Smaller droplet sizes and higher levels of prevaporization are required.) Introduction of some initial vapor fuel or heating of the detonation tube extends the droplet size limits at which near-full performance is obtained. More generally, results suggest that, for small enough droplets and/or with sufficient prevaporization of the fuel, liquid-fueled PDEs will provide comparably efficient single-cycle propulsive performance to gaseous fueled PDE devices.

Nomenclature

A	=	cross-sectional area of detonation tube
B_i	=	transfer number of the ith droplet
C_{Di}	=	drag coefficient of the ith droplet
c_p	=	heat capacity of the gas at constant pressure
$c_{p,v}$	=	heat capacity of the fuel vapor at constant pressure
c_v	=	heat capacity of the gas at constant volume
d_{pi}	=	diameter of the ith droplet
d_{p0}	=	initial droplet diameter
d_{tube}	=	diameter of the detonation tube
F_{conv}	=	correction to the droplet vaporization rate due to convective flow effects
$h_{v,f}$	=	enthalpy of the fuel vapor
I	=	impulse
$I_{\text{sp},f}$	=	fuel-based specific impulse
$I_{\text{sp,mix}}$	=	mixture-based specific impulse
L	=	latent heat of vaporization of the fuel
M	=	local droplet mass per unit volume
$\dot{M}$	=	local droplet mass vaporization rate per unit volume
$\dot{m}_i$	=	mass of the ith droplet
$\dot{m}_i$	=	mass vaporization rate of the ith droplet
P_0	=	ambient pressure
P_3	=	pressure at the head-end wall
p	=	pressure
q	=	heat release
R^0	=	universal gas constant
$\boldsymbol{S}_D$	=	droplet drag effects on the gas source term
S_E	=	work and heat flux effects of the droplets on the gas source term
S_{Ev}	=	internal and kinetic energy transfer source term
$\boldsymbol{S}_v$	=	momentum transfer between the droplets and the gas source term
S_ρ	=	mass addition due to droplet vaporization source term
S_Ω	=	chemical reaction source term
T	=	temperature
T_{si}	=	surface temperature of the ith droplet
t	=	time
W_i	=	molecular weight of species i
$\bar{W}$	=	average molecular weight of the gas
$\boldsymbol{V}$	=	droplet velocity
$\boldsymbol{v}$	=	gas velocity
$\boldsymbol{X}$	=	droplet position
Y_i	=	mass fraction of species i
γ	=	ratio of specific heats, c_p/c_v
η	=	liquid fuel fraction
λ	=	thermal conductivity
ν	=	scaled stoichiometric coefficient
ν_i	=	stoichiometric coefficient of species i
ρ	=	gas-phase density
ρ_i	=	gas-phase density of species i
ρ_ℓ	=	density of the liquid fuel
ϕ	=	equivalence ratio

Introduction

In recent years there has been much interest in the potential of pulse detonation engines (PDEs). Potential benefits of PDE devices include their relative simplicity, efficient performance, and ability to operate over a wide range of speeds.[1] In practice, many propulsion applications will be weight and volume limited and will, therefore, require the use of a liquid fuel to be viable. However, even the detonability of many practical low vapor-pressure liquid fuels such as JP-10 has been questioned. Therefore, it is important to investigate the feasibility of PDE operation with such liquid fuels and to compare their performance to those utilizing gaseous fuels.

On a fundamental level, systematic investigations into the detonation of liquid fuel mixtures can be traced back to the early 1960s when experimental work by Webber[2] and Cramer[3] appeared in the literature, as did a theoretical analysis by Williams.[4] Over the years, work has continued, with particular attention being focused on such issues as fuel droplet size effects[4–6] and droplet shattering and shearing effects on detonation propagation[7] and ignition.[8] The importance of some initial fuel vapor for the initiation and sustenance of liquid-fueled detonation has been noted by several authors.[9–11] Bar-Or et al.,[12] in their study of cylindrical liquid-fueled detonations of both high and low vapor pressure, further note such a requirement, and report more general qualitative differences between multiphase detonation of high and low vapor-pressure fuels. Papavassiliou et al.[13]

Received 25 June 2004; revision received 8 December 2004; accepted for publication 3 January 2005.

*Research Mathematician, Code 6410, Center for Reactive Flow and Dynamical Systems. Member AIAA.
†Head, Code 6410, Center for Reactive Flow and Dynamical Systems. Fellow AIAA.

additionally found that detonation of 5-μm decane droplets resulted in a cell size almost twice as large as that for a fully vaporized decane–air mixture, suggesting a similar increase in the initiation energy needed for liquid fuel detonation.

Beyond the determination of such fundamental detonability and stability issues accompanying the use of liquid fuel, research and development of such detonation propulsion systems involves selecting and determining the performance of various device components such as inlets, combustors (detonation tubes), and nozzles.[14] In the present work, the emphasis is only on one key component of the overall device, the thrust tube or detonation tube. Furthermore, attention is focused on the single-cycle operation of an idealized thrust tube, which consists of a tube closed at one end and open at the other. There have been many studies on propulsive performance of this idealized PDE operating on gaseous fuels.[15–23] Correlations predicting performance have been derived based on numerical,[19] theoretical,[22] and experimental[23] work. Reviews of the available information have been provided by Kailasanath.[24,25]

Although numerous detailed studies on the operation and performance of gaseous-fueled pulse detonation devices have been made, very little information has been published on the additional complications of operation with liquid fuels[11,26] and the impact it would have on even the single-cycle performance. One recent study involving liquid fuel was that of Fan et al.[27] They experimentally investigated the detonation of a liquid C_8H_{16}–air mixture in a detonation tube and obtained a correlation for predicting impulse. In their experimental setup, fuel is injected into a mixing zone rather than directly into the detonation chamber. Their results suggest that liquid fuels are tenable for practical applications. However, heating of the mixing chamber may have resulted in a purely gaseous fuel–oxidant mixture being injected into the detonation chamber so that their results may be more accurately a reflection of a prevaporized mixture. Experimentally, detonability of fine JP-10 fuel droplets in air with some amount of fuel vapor has been demonstrated by Brophy et al.[11] To investigate the effect of liquid-fuel characteristics on propulsive performance in more detail, in the current work we numerically simulate detonations in a tube to obtain propulsive performance estimates of an idealized PDE. The fuel we consider is JP-10, and for the oxidant inside the tube, we consider first O_2 and then air. Results for several droplet sizes and levels of prevaporization are presented.

Model

The numerical model we use in our simulations is based on an Eulerian–Lagrangian formulation of gas–droplet interactions. More specifically, in our model governing equations for the gas phase are the Euler equations, with modifications via source terms to account for the multiphase nature of the flow. Gas-phase equations are solved using a flux-corrected transport algorithm,[28] a conservative, monotonic algorithm with fourth-order phase accuracy. Droplet equations are solved in a Lagrangian frame of reference and describe the position, velocity, temperature, and vaporization of each droplet in the simulation. Thus, our model includes two-way coupling between the gas and droplet phases: The equations for each droplet depend on local gas-phase conditions, and source terms in the gas-phase governing equations account for droplet effects on the gaseous flow. Droplet temperature is calculated using an infinite conductivity model, and convective effects on droplet vaporization and heating are taken into account. For numerical tractability, we allow each droplet explicitly solved for in our simulation to represent a group of virtual droplets, each of which is assumed to behave identically to the tracked droplet and is located within the same computational cell. Typically, we track approximately 75,000–150,000 droplets per simulation, with the corresponding number of virtual droplets determined by the droplet size, tube volume, and overall mixture equivalence ratio. In the present simulations, attention will be focused on smaller sized droplets. As a result, droplet breakup, shearing, and deformation may be considered negligible. More generally, the formulation is based on the assumption that the system is dilute. (In the present calculations, indeed, the droplet volume fraction is $< 5 \times 10^{-4}$ for O_2 and $< 6 \times 10^{-5}$ for air.) Thus, particle–particle interactions may be considered negligible. Monodisperse droplet distributions are considered, and droplets are randomly seeded in such a way that their overall distribution in the tube should be approximately uniform.

Gas-phase equations take the form

$$\frac{\partial \rho}{\partial t} + \nabla \cdot \rho \boldsymbol{v} = S_\rho \tag{1}$$

$$\frac{\partial \rho_F}{\partial t} + \nabla \cdot \rho_F \boldsymbol{v} = S_\rho - S_\Omega \tag{2}$$

$$\frac{\partial \rho_X}{\partial t} + \nabla \cdot \rho_X \boldsymbol{v} = -\nu S_\Omega \tag{3}$$

$$\frac{\partial \rho_I}{\partial t} + \nabla \cdot \rho_I \boldsymbol{v} = 0 \tag{4}$$

$$\frac{\partial \rho_{pi}}{\partial t} + \nabla \cdot \rho_{pi} \boldsymbol{v} = \nu_{pi} S_\Omega \tag{5}$$

$$\frac{\partial \rho \boldsymbol{v}}{\partial t} + \nabla \cdot \rho \boldsymbol{v}\boldsymbol{v} + \nabla p = \boldsymbol{S}_D + \boldsymbol{S}_v \tag{6}$$

$$\frac{\partial E}{\partial t} + \nabla \cdot E \boldsymbol{v} + \nabla \cdot p \boldsymbol{v} = S_E + S_{Ev} + q S_\Omega \tag{7}$$

where ρ is the total gas-phase density and $\boldsymbol{v}$ is the gas-phase velocity. The density of the gaseous fuel is $\rho_F = \rho Y_F$, $\rho_X = \rho Y_X$ is the (gaseous) O_2 density, $\rho_I = \rho Y_I$ is the species density of N_2, and $\rho_{pi} = \rho Y_{pi}$ is the density of product $i = 1, 2$ (here CO_2 and H_2O). Total energy density $E = e + \frac{1}{2}\rho|\boldsymbol{v}|^2$ in which the internal energy density $e = p/(\gamma - 1)$. Gas-phase temperature will be determined from the equation of state $p = \rho R^0 T/\bar{W}$. We assume that specific heats are constant and that viscosity and thermal conductivity vary with temperature according to Sutherland's expression.

Source terms appearing on the right-hand sides of the equations account for fuel droplet effects. Because droplets are modeled using a Lagrangian tracking approach, although not explicitly denoted here, all source terms should be considered as summations over the droplets local to each computational cell of the simulation. Source terms take the following form:

$$S_\rho = \dot{M} \tag{8}$$

$$\boldsymbol{S}_D = -M \frac{\mathrm{d}\boldsymbol{V}}{\mathrm{d}t} \tag{9}$$

$$\boldsymbol{S}_v = \dot{M} \boldsymbol{V} \tag{10}$$

$$S_E = -M \boldsymbol{V} \cdot \frac{\mathrm{d}\boldsymbol{V}}{\mathrm{d}t} - \frac{\dot{M} c_p}{B}(T - T_s) \tag{11}$$

$$S_{Ev} = \dot{M} h_{v,f} + \frac{1}{2}\dot{M}|\boldsymbol{V}|^2 \tag{12}$$

Here S_ρ is the addition of mass to the gas phase due to vaporization of the fuel droplets. Vaporization increases both the total gas density ρ and the gaseous fuel density ρ_F. $\boldsymbol{S}_D$ is the drag on the gas phase due to the droplets and $\boldsymbol{S}_v$ the momentum transferred to the gas phase due to the newly vaporized fuel. The energy source term S_E accounts for the work done by the droplets on the gas and the heat flux from the gas to the droplets. S_{Ev} accounts for the enthalpy and kinetic energy addition to the gas due to the newly vaporized fuel. The enthalpy term takes the form $h_{v,f} = c_{p,v} T_s$, where $c_{p,v}$ is the specific heat of the fuel vapor and T_s is the surface temperature of the vaporizing droplet. S_Ω represents the consumption of fuel and oxidant due to combustion, and the parameter ν is a scaled stoichiometric coefficient, $\nu = \nu_X W_X / \nu_F W_F$, with ν_{pi} scaled stoichiometric coefficients of the products. We assume only vapor-phase combustion, that is, direct droplet burning is not specifically considered. Chemical reaction is modeled through a two-step induction parameter model,[29] in which a reaction progress variable that tracks how long fuel vapor has resided in a given computational cell is convected in addition

to the flowfield variables. This variable is accumulated based on the induction time correlation for JP-10 determined by Davidson et al.[30] Once the chemical induction time has elapsed, energy release begins, the magnitude of which depends on the specific mixture/reaction. This value depends on the stoichiometric ratio and is calibrated using the chemical equilibrium compositions (CEC) code[31] such that the correct gaseous Chapman–Jouguet (C–J) detonation velocity is obtained. Energy release after the induction time has elapsed is distributed over a characteristic time, which corresponds to 5% of the total energy available being released per time step. In all of the calculations discussed here, the overall fuel–oxidant mixture is at stoichiometry, $\phi = 1$. This corresponds to an initial fuel mass fraction (gas plus liquid) in the seeded droplet region of $Y_{F0} = 0.23$ when the oxidant is O_2 and $Y_{F0} = 0.063$ when the oxidant is air. The heat release of the chemical mechanism then is $q = 2.46 \times 10^{11}$ erg/g for JP-10–O_2 and $q = 5.21 \times 10^{11}$ erg/g for JP-10–air.

Equations governing the ith droplet's velocity $\boldsymbol{V}_i(t)$, position $\boldsymbol{X}_i(t)$, temperature $T_{si}(t)$, and diameter $d_{pi}(t)$, in a Lagrangian frame of reference, are given by

$$\frac{\mathrm{d}\boldsymbol{V}_i}{\mathrm{d}t} = \frac{3}{4}\frac{\rho}{\rho_\ell}\frac{C_{Di}}{d_{pi}}|\boldsymbol{v} - \boldsymbol{V}_i|(\boldsymbol{v} - \boldsymbol{V}_i) \tag{13}$$

$$\frac{\mathrm{d}\boldsymbol{X}_i}{\mathrm{d}t} = \boldsymbol{V}_i(t) \tag{14}$$

$$m_i\, c_\ell \frac{\mathrm{d}T_{si}}{\mathrm{d}t} = \frac{\dot{m}_i c_p}{B_i}(T - T_{si}) - \dot{m}_i L \tag{15}$$

$$\frac{\mathrm{d}d_{pi}^2}{\mathrm{d}t} = -\frac{8\lambda}{\rho_\ell c_p}\,\ell_n(1 + B_i)F_{\mathrm{conv}} \tag{16}$$

Density of the liquid droplet is ρ_ℓ. Parameters appearing in the preceding equations include the droplet drag coefficient C_{Di} and the transfer number B_i. For high values of Reynolds number, the drag coefficient is chosen to be of the form of that by Igra and Takayama[32]:

$$\log_{10}(C_D) = 7.8231 - 5.8137\log_{10}(Re_p) + 1.4129[\log_{10}(Re_p)]^2 - 0.1146[\log_{10}(Re_p)]^3 \tag{17}$$

For smaller Reynolds numbers the drag coefficient of Schiller and Naumann is used[33]:

$$C_D = 24\left(1 + 0.15Re_p^{0.687}\right)\Big/ Re_p \tag{18}$$

The transfer number depends on the local mass fraction at the droplet surface, obtained from the Clausius–Clapeyron relation. The factor F_{conv} is a correction to the droplet evaporation rate due to convective effect, taken to be of the form given by Faeth and Lazar[34]:

$$F_{\mathrm{conv}} = 1.0 + \frac{0.278(Re_p)^{\frac{1}{2}}Pr^{\frac{1}{3}}}{\left(1.0 + 1.232\Big/ Re_p Pr^{\frac{4}{3}}\right)^{\frac{1}{2}}} \tag{19}$$

The droplet mass rate of change $\dot{m}$ is based on the classical spherically symmetric quasi-steady derivation[35] with this correction. More details about the model formulation and its validation and verification may be found in Ref. 36.

The geometry we choose to model is that of an idealized PDE consisting of a single tube closed at one end, open at the other, surrounded by air. Current calculations are for an axisymmetric geometry in which the detonation tube is 1 m in length, and the tube diameter $d_{\mathrm{tube}} = 4$ cm. To initiate the detonation, initially a 1-cm high-pressure driver region exists at the left end of the tube, and to the right of the diaphragm at $z = 1$ cm is a 4-cm gaseous initiation region of (stoichiometric) fully vaporized JP-10 in oxygen. Immediately adjacent to the gaseous initiation region, the remaining section of the tube contains randomly seeded fuel droplets in oxygen or air. Outside of the tube the air is at 298 K. Extension of the computational domain to the region outside of the tube removes the difficulty of appropriately choosing boundary conditions[37] at the open end of the tube (because it is no longer a computational boundary). The grid is extended well beyond the tube boundaries, and far from the tube, the grid is stretched such that boundary conditions at the edge of the domain should have negligible effect on the flow within the tube and thereby the flow parameters used to obtain performance estimates. Near the tube and inside of it, the grid resolution we use is $\mathrm{d}z = \mathrm{d}r = 0.025$ cm. The simulation time-step size is $\mathrm{d}t = 1.0 \times 10^{-8}$ s, which is sometimes increased near the end of the run when the detonation has long left the tube and conditions inside of the tube are relaxing to the ambient condition. Resolution tests show that such discretizations and time-step sizes are sufficient for accurately determining basic detonation structure and PDE performance measures.

In the next two sections, we begin by discussing numerical simulation results describing detonation structure and performance for JP-10 fuel droplets in oxygen because a wider operating regime is possible for O_2 as compared to air. Following this discussion, performance results for JP-10 fuel droplets in air are presented. Summary comments and conclusions then follow.

Liquid-Fueled Detonations: JP-10–O_2

To investigate propulsive performance of liquid-fueled PDEs, we first numerically simulate detonation of fully prevaporized JP-10 in O_2, fully liquid JP-10 with initial droplet diameter $dp_0 = 10$ μm and with $dp_0 = 20$ μm and $dp_0 = 20$ μm JP-10 droplets in a tube in which the liquid fuel fraction $\eta = 0.8$ and $\eta = 0.9$. Typical flowfield results are shown in Figs. 1–4. In Fig. 1, profiles of pressure at several fixed locations within the detonation tube are shown vs time for the simulation in which all fuel is initially provided in droplet form with $dp_0 = 10$ μm. Here at all downstream locations, we see the pressure

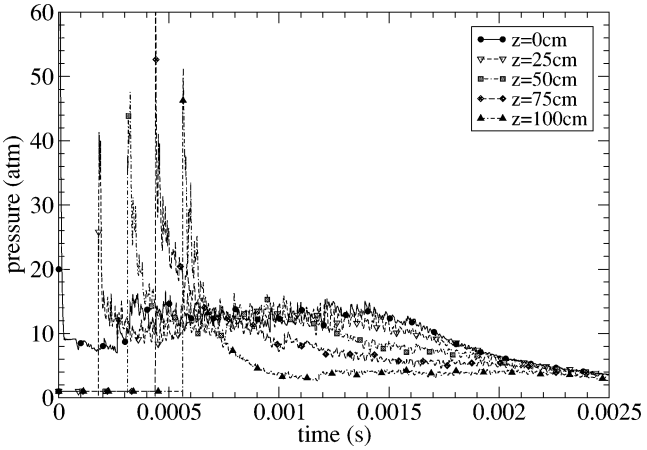

Fig. 1 Pressure vs time, at several fixed locations within the detonation tube: JP-10–O_2 with all ambient fuel initially provided as droplets with initial diameter $dp_0 = 10$ μm, $T_{\mathrm{amb}} = 298$ K.

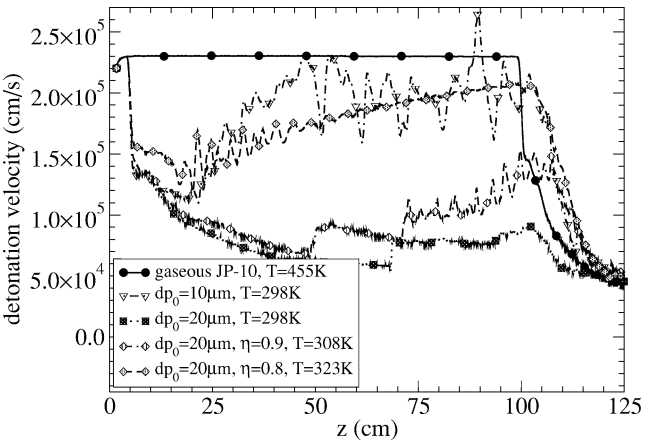

Fig. 2 JP-10–O_2 detonation front velocity vs axial front location, as the detonation propagates down the tube.

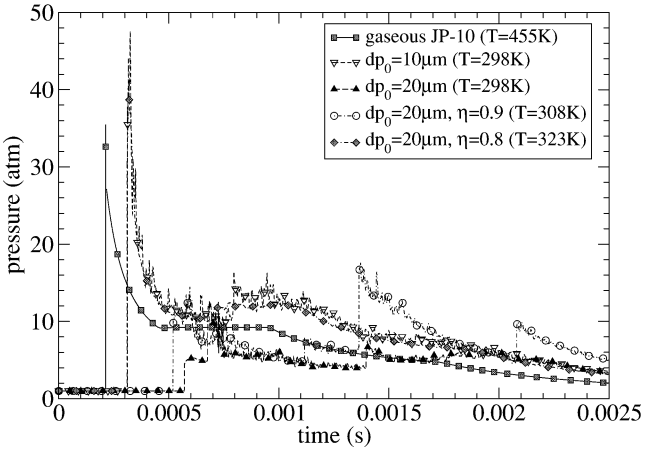

Fig. 3 Pressure vs time, at $z = 50$ cm, JP-10–O_2 with several different forms of initial fuel.

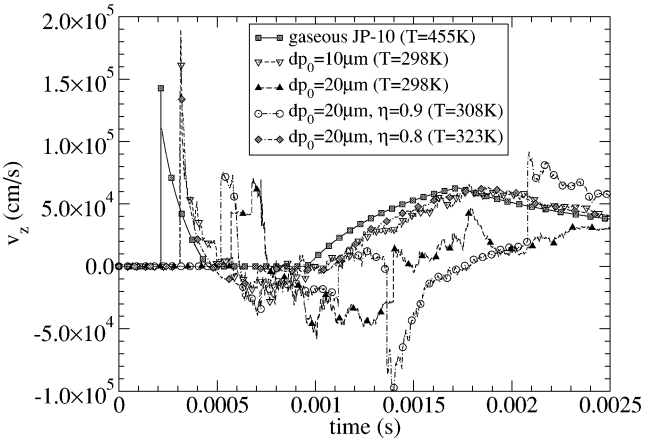

Fig. 4 Gas-phase axial velocity v_z vs time, at $z = 50$ cm, JP-10–O_2 with several different forms of initial fuel.

is initially at the ambient condition of 1 atm. When the detonation wave passes each diagnostic location, the pressure jumps abruptly to a high value. After the front passes by, the pressure relaxes to a near steady plateau pressure at each point. When the detonation leaves the tube at about time = 0.6 ms, a disturbance propagates back toward the head end of the tube in the form of a reflected expansion wave. As this expansion wave reaches each diagnostic location, the pressure begins to decrease and decays toward the ambient pressure. The various observations made here are very similar to those observed in operations with gaseous fuels (as, for example, in Ref. 19). Note, however, that results here for liquid fuel are noisier than numerical simulation results for fully vaporized fuel. This is because, when the fuel is in liquid form, energy release is discontinuous. Resulting waves interact with one another as well as the tube surface causing the noise.

In Fig. 2, results of detonation front velocity vs time is shown for each case. (Front velocity shown here was calculated at the radial midpoint; the oscillatory nature of the velocity is due in part to time-dependent corrugation of the front.) In all simulations, a steady detonation develops within the short 5-cm region of fully vaporized JP-10 and begins propagating at the C–J detonation velocity of 2300 m/s. For the fully vaporized case, the detonation front continues at this velocity down the remaining section of the tube. However, when some of the fuel is provided in liquid form, once the section of the tube containing droplets is reached, the detonation velocity immediately decays. This is a result of fuel vapor no longer being immediately available for chemical reaction, coupled with the well-known attenuation effect of a dispersed phase. For the detonation to survive, this attenuation effect must be overcome. If the droplets vaporize rapidly and the subsequent energy release couples with the leading shock wave, a propagating detonation will result.[36] Indeed, as the leading shock wave continues to propagate into the droplet mixture, the mixture temperature begins to rise, and the fuel droplets are heated and begin to vaporize, providing the needed gaseous fuel combustion to sustain a detonation. Smaller droplets more quickly heat and vaporize and, thus, more quickly transition to a fully coupled self-propagating detonation structure. (Note the $dp_0 = 10$ μm result in Fig. 2.) The existence of some initially vaporized fuel immediately available for chemical reaction likewise speeds and smoothens transition to a self-sustained propagating detonation wave. (For example, see the curve for liquid fuel fraction $\eta = 0.8$ in Fig. 2.)

When a near-C–J propagating detonation structure does not immediately form in the ambient section of the tube, qualitative differences in the flowfield within the tube result. Graphs showing how pressure and gas velocity within the tube differ are shown in Figs. 3 and 4. In Fig. 3, results of pressure vs time at the axial midpoint $z = 50$ cm of the tube are shown for each of the simulations. In Fig. 4, the axial velocity v_z is shown vs time at the same location. More details of the simulation of multiphase detonations in tubes, including dependence on model parameters, has been discussed elsewhere.[36] In the present work, the emphasis will be on performance of an idealized PDE.

Performance Results

To evaluate the single-cycle performance of JP-10–O_2-fueled PDEs, we calculate head-end pressure, specific impulse, and fuel-based specific impulse for each of the simulation cases mentioned earlier. Results showing the pressure at the head-end of the detonation tube (which is proportional to the thrust) are given in Fig. 5, where here and subsequently data shown correspond to flowfield variable quantities at the radial midpoint $r = 1$ cm. (Propulsive measures calculated using head-end data at the radial axis or endpoint result in virtually identical results.) For fully vaporized JP-10, we see the standard gaseous detonation result of the head-end pressure jumping to a constant plateau value (here ~9.23 atm) after the passage of the detonation wave, followed in time by a slow relaxation to ambient conditions. When the fuel is provided in the form of liquid 10-μm droplets, the head-end pressure initially decays slightly before jumping back up to a value that averages to about 12.9 atm. (The reason for the different values in the plateau pressure is discussed later.) Presence of the droplets results in the head-end pressure being much more noisy than for the fully vaporized case. When droplets of size $dp_0 = 20$ μm without any prevaporized fuel are used, we see a longer and deeper decay in the head-end pressure near the beginning of the simulation. After about 0.8 ms, the head-end pressure jumps significantly to about 7.5 atm, but is still noticeably below the plateau pressure reached when droplets of size $dp_0 = 10$ μm are used. When 20% of the 20-μm droplet liquid fuel is prevaporized ($\eta = 0.8$), however, the head-end pressure initially decays in time but then quickly and relatively smoothly increases toward a

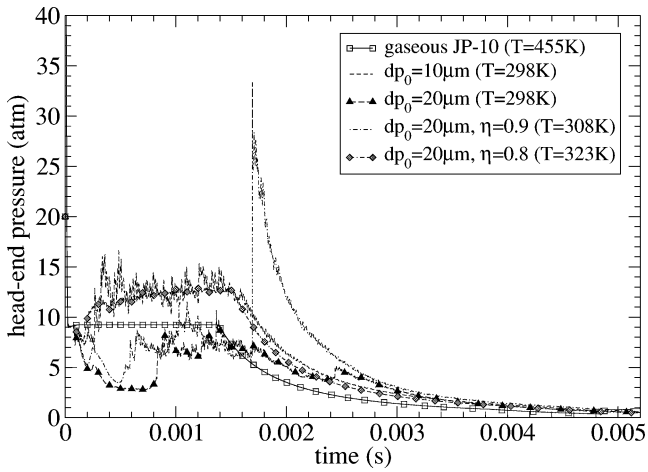

Fig. 5 Head-end pressure vs time, JP-10–O_2.

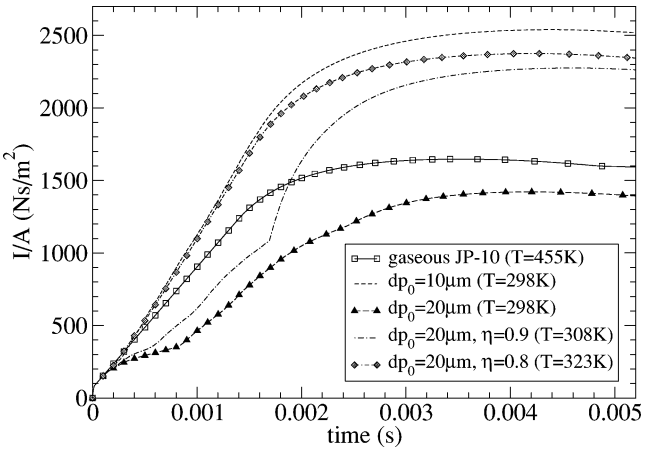

Fig. 6 Normalized impulse vs time, JP-10–O_2.

plateau value similar to that seen for 10-μm droplets. When a lesser amount of the fuel is prevaporized, or less mixture heating has taken place such that the initial liquid fuel fraction is $\eta = 0.9$, we see a markedly different response. Here an initial decay comparable to that for 20-μm droplets with no prevaporization occurs, followed by a similar, but earlier in time, jump to a head-end pressure of 7–8 atm. However, when 10% of the fuel is prevaporized, a little bit later in time, at about 1.69 ms, we see a huge jump in the head-end pressure to ~33 atm, followed immediately by a relaxation to ambient conditions. To compare the various cases, a normalized impulse per unit area, defined as

$$\frac{I}{A} = \int (P_3 - P_0)\,\mathrm{d}t$$

where A is the surface area of the head-end wall, P_3 is the head-end pressure, and P_0 is the atmospheric pressure, is shown in Fig. 6. At first glance, the results shown in Fig. 6 may be surprising because some of the performance results with liquid fuels are higher than with the gaseous fuel. However, this is because the amount of fuel is different between some of the cases. More specifically, this is because, for the cases considered with fully and partially vaporized JP-10, the ambient temperature in the tube must be greater than 298 K for such vapor to exist at standard pressure. In the fully vaporized simulation, therefore, we stipulate that the ambient temperature inside the tube is at the boiling point of JP-10, $T_b = 455$ K. For the partial vaporization simulations, we calculate the ambient temperature, which results in gas–vapor equilibrium at the droplets' surfaces using the Clausius–Clapeyron relation. The higher temperature required at the ambient pressure of 1 atm when some or all of the fuel is prevaporized results in a corresponding decrease in density of the mixture such that the total mass of fuel in the tube decreases as the level of prevaporization increases in our simulations because we hold the equivalence ratio fixed at $\phi = 1$. Thus, even for comparably efficient performance, plateau pressures in Fig. 5 (and, thus, also measures such as thrust and impulse) are expected to vary with initial ambient temperature. When such measures are normalized to account for the differing fuel masses, such as in the fuel-based specific impulse, defined as the impulse divided by the weight of the fuel $I_{\mathrm{sp},f} = I_{\mathrm{sp}}/m_f g$, results become more directly comparable. Fuel-based specific impulse is shown in Fig. 7. Here, the limiting (highest) value is indeed observed for the fully vaporized gaseous JP-10.

More specifically, what our simulations reveal is that, in terms of fuel-based specific impulse, there is little if any degradation in performance resulting from the use of liquid fuels. Note that, in Fig. 7 of fuel-based specific impulse, simulations with gaseous JP-10, droplets of size $dp_0 = 10$ μm, and $dp_0 = 20$ μm droplets with $\eta = 0.8$ all are giving very similar values of $I_{\mathrm{sp},f}$. (See also Table 1.) When fuel is provided in droplet form, however, it takes more time for maximum impulse to be achieved. In Figs. 3 and 4, we see that the structure of the detonation for these two liquid-fueled cases is

Table 1 Performance results for JP-10–O_2

Mixture	Percentage of fully vaporized JP-10–O_2 $I_{\mathrm{sp},f}$, %[a]
$dp_0 = 10$ μm in O_2, $\eta = 1.0$	97.4
$dp_0 = 20$ μm in O_2, $\eta = 1.0$	54.5
$dp_0 = 20$ μm in O_2, $\eta = 0.9$	90.6
$dp_0 = 20$ μm in O_2, $\eta = 0.8$	99.6

[a]Percentage shown is the maximum fuel-based specific impulse, as compared to the fully vaporized JP-10–O_2 maximum fuel-based specific impulse.

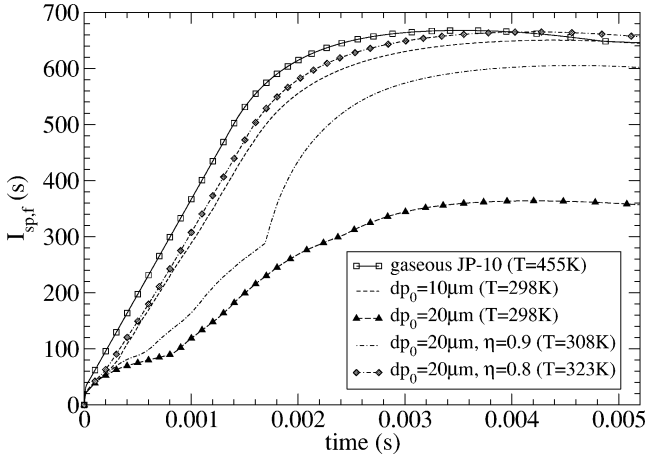

Fig. 7 Fuel-based specific impulse vs time, JP-10–O_2.

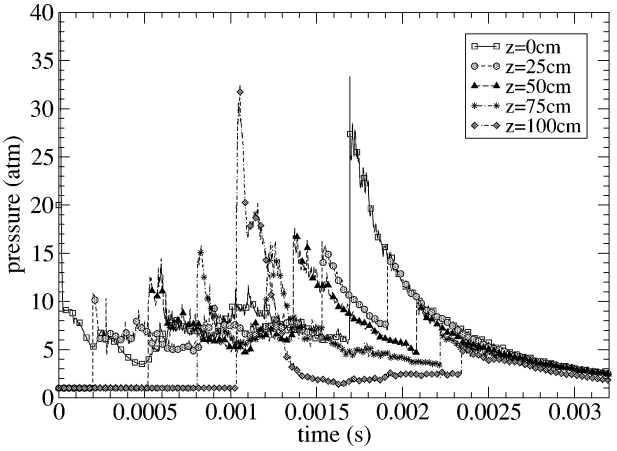

Fig. 8 Pressure vs time at several fixed locations within the detonation tube: JP-10–O_2 and ambient liquid-fuel fraction $\eta = 0.9$ with liquid droplets of initial size $dp_0 = 20$ μm and $T_{\mathrm{amb}} = 308$ K.

not dissimilar to that of the gaseous JP-10 detonation. However, a marked decrease in $I_{\mathrm{sp},f}$ is observed when droplets of $dp_0 = 20$ μm without any prevaporized fuel are utilized. Here the maximum $I_{\mathrm{sp},f}$ is just over half of that obtained for gaseous JP-10. Figures 2–4 suggest the reason for this degradation. When fuel is provided as 20-μm droplets with no prevaporization, sufficient development of the detonation does not occur in the 1-m tube, evidenced by the low front velocity and lower pressure values at the front as compared to the fully developed gaseous case. Significant fuel exits the tube unburnt. However, if even a small amount of prevaporized fuel is provided, that is, enough such that energy release is fully coupled to the detonation front before it leaves the tube, a marked improvement in performance results. For the case of 20-μm droplets with $\eta = 0.9$, for example, we see a similarly low front velocity and weak pressure waves through most of the tube. However in this case, near the end of the tube significant energy release has begun, evidenced in part by the increasing front velocity shown in Fig. 2. A rise in pressure at the detonation front when it is near the end of the tube, which likewise indicates this transition, is shown in Fig. 8. Figure 8, which shows

pressure vs time at several fixed locations within the tube, also reveals that near the end of the tube, a strong pressure wave is reflected back toward the closed end of the tube. This reflected wave causes the spike in the head-end pressure seen in Fig. 5 at time ~0.0017 s. Fuel-based specific impulse for this case approaches about 90% of that achieved with fully prevaporized JP-10. That comparable performances are achieved for liquid fuels as long as detonation takes place somewhere within the tube is a result similar to that obtained by Harris et al.[38] for gaseous fuels in which detonation initiation occurred either very rapidly near the closed end or occurred much later nearer the open end of the tube. Their head-end pressure and impulse measurements are qualitatively similar to those observed here.

Results for JP-10–Air

With the encouraging results just shown, attention is now shifted to simulation of idealized PDEs operating with JP-10–air mixtures. Only about 30% of the fuel can exist stably in a vapor state at 298 K when air is the background medium. Therefore, this condition was used as a baseline in our study of droplet size effects. In Fig. 9 detonation velocities for several initial droplet sizes and prevaporization levels are shown. Here we see similar trends as for JP-10–O_2 in that propagation near the gaseous JP-10–air C–J velocity of 1786 m/s is possible for a range of small initial droplet sizes. Criticality depends on the ambient temperature/prevaporization level, just as we saw for JP-10–O_2 mixtures. Note that for droplets in air, however, the constraint on droplet size for achieving sustained near-C–J propagation is much stricter than it is for oxygen. Whereas for oxygen mixtures the critical droplet diameter for steady propagation at 298 K is between $dp_0 = 10$ and 20 μm, for air mixtures even $dp_0 = 5$ μm is too large to sustain a near-C–J front velocity. We also observe that, whereas Fig. 2 indicates gradual asymptoting to an equilibrium, velocity may occur down the entire tube length, or that the process of transition to a near-C–J velocity may occur near the end of the tube as a series of sudden jumps in front velocity, our PDE simulations with JP-10–air suggest that if such a transition has not occurred fairly near the beginning of the tube (within ~30 cm) it most likely will not occur at all.

In terms of performance, as we might expect, head-end pressure plateaus at a lower value for air than for oxygen, but again overall droplet size trends are similar to the ones described for JP-10–O_2. Representative head-end pressures for JP-10–air are shown in Fig. 10 for four droplet sizes, $dp_0 = 1$, 3, 4, and 5 μm. There is very little difference in head-end pressure for the 1- and 3-μm cases, but as droplet size increases, significant loss results even for the $dp_0 = 4$ μm droplet case. Impulse buildup (Fig. 11) likewise is a problem when $dp_0 = 4$ and 5 μm at this level of prevaporization ($\eta = 0.7$), indicating that much smaller droplets are needed for airbreathing operation than for oxygen.

The impact of initial prevaporization level on the computed performance is illustrated by Fig. 12, where the fuel-based specific

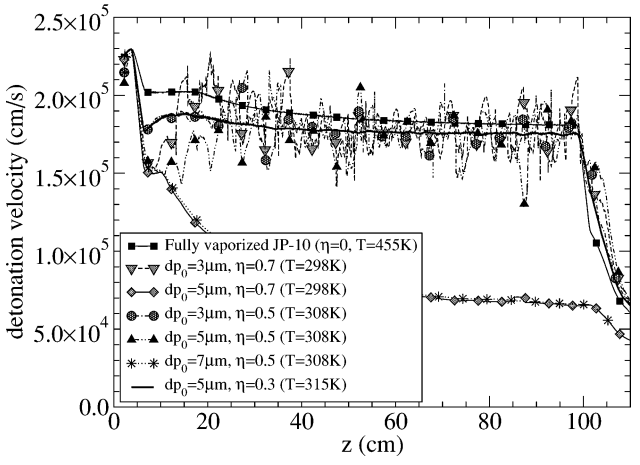

Fig. 9 Detonation front velocity vs time for JP-10–air for several initial fuel droplet sizes and prevaporization levels.

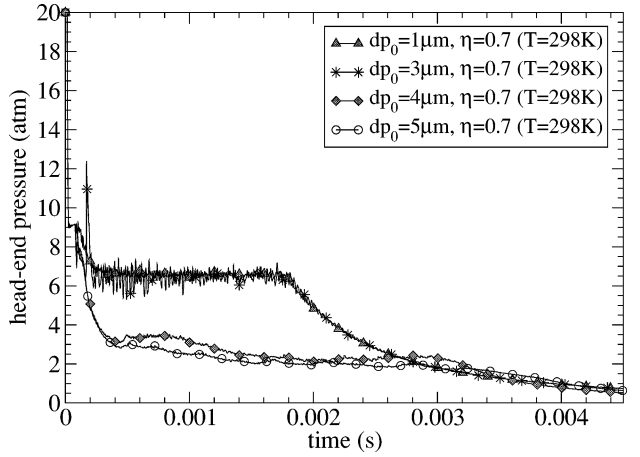

Fig. 10 Head-end pressure vs time for JP-10–air for several different initial fuel droplet sizes.

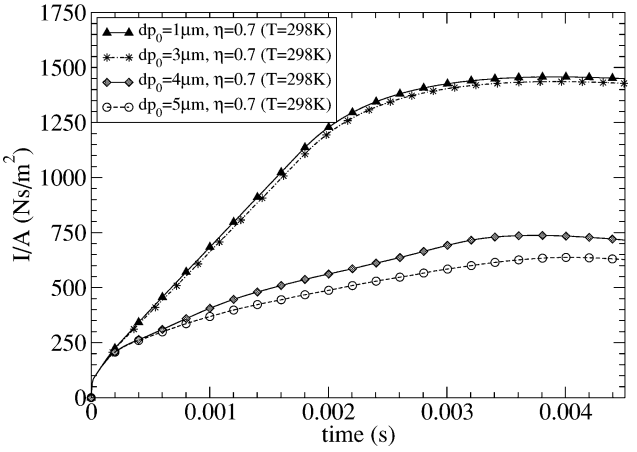

Fig. 11 Normalized impulse vs time, JP-10–air.

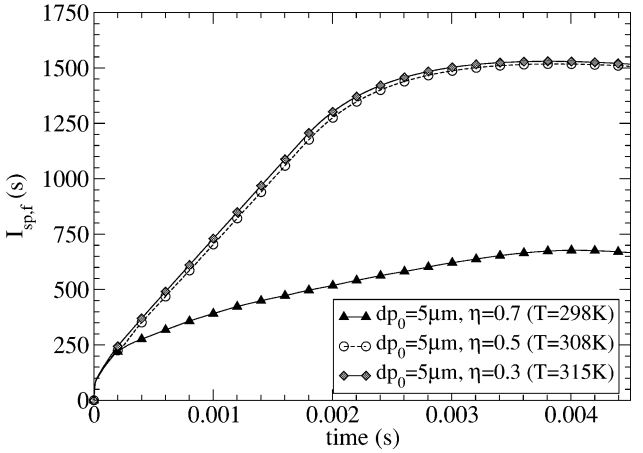

Fig. 12 Fuel-based specific impulse vs time for JP-10–air.

impulse is shown for three cases in which the initial droplet size is maintained constant at $dp_0 = 5$ μm but the level of prevaporization is varied from 30% ($\eta = 0.7$) to 70% ($\eta = 0.3$). Less than half of the expected performance is attained with only 30% prevaporization, as compared to the higher levels.

Comparisons with Previous Observations

Whereas experimental data of liquid JP-10 detonation suitable for comparison with our results are quite scarce, limited data exist with which a few comparisons can be made. Brophy and coworkers, for

example, have experimentally measured front velocities of liquid JP-10 detonation (C. Brophy, private communication, 2002). They found that, for JP-10–O_2 with $\phi \sim 1$, $dp_0 \sim 11$ μm and $\eta > 0.985$ detonation velocities at the tube end averaged out to near 2250 m/s (+240 m/s −209 m/s). For JP-10–air mixtures with $\phi \sim 1.25$, $dp_0 \sim 3$ μm, $\eta \sim 0.3$ detonation velocities at the end of the tube averaged out to be near 1740 m/s +65 m/s −56 m/s. These results are comparable to those obtained in our calculations, as evidenced by Figs. 2 and 9 showing detonation velocity in the tube for JP-10-O_2 and JP-10–air respectively (where $\phi = 1.0$).

With respect to liquid-fuel detonability characteristics, we see that, qualitatively similar to the results shown by our numerical simulations, experiments show that small droplet sizes and the existence of some initial fuel vapor increase a mixture's detonability. Brophy et al.[11] for example have experimentally investigated the detonability of liquid JP-10–air mixtures with an overall equivalence ratio of $\phi = 1.5$. In a continuous airflow PDE geometry with a JP-10–oxygen predetonator as the initiator, they found that droplets with diameter below about 3 μm and/or a large fraction of fuel vapor present are required for successful detonation. Bull et al.[9] studied unconfined detonation of both high and low vapor pressure fuels and similarly concluded that for larger droplet sizes a certain quantity of initial fuel vapor may be required for sustained detonation propagation.

In terms of propulsive performance data, although we know of no experimental data for liquid JP-10, various theoretical estimates exist for vapor-phase fuel. Kailasanath et al.,[19] for example, provide a general correlation. Wintenberger et al.[22] have provided theoretical estimates and show results from their correlation for fully vaporized JP-10 detonation in both air and oxygen. Our numerical calculations for fully vaporized JP-10–O_2 result in a maximum specific impulse per unit area of about 1647 $N \cdot s/m^2$, and for fully vaporized JP-10–air ~947 $N \cdot s/m^2$, generally comparable to those predicted by the correlation of Kailasanath et al.[19] In terms of mixture-based specific impulse, when the detonation is fully developed within the tube our liquid fuel simulations yield $I_{sp,mix} \sim 151$–155 s for JP-10–O_2 and $I_{sp,mix} \sim 112$–116 s for JP-10–air, comparable also to the analytical gaseous predictions of Wintenberger et al.[22]

Conclusions

Numerical simulations of liquid-fueled detonation of JP-10 mixtures in an idealized PDE geometry have been made and propulsive performance measures computed. We find that, when detonation is fully developed within the detonation tube, liquid-fuel detonation in both air and oxygen is comparably efficient to detonation of the fully vaporized fuel mixture. We note that impulse I is larger for liquid fuel in which detonation has fully developed within the tube. This is due to the larger mass of fuel at ambient pressure available for chemical reaction. In terms of maximum fuel-based specific impulse, performance results are very similar regardless of how the fuel is provided as long as full transition to detonation occurs within the tube. Time-dependent thrust, however, may vary significantly depending on the initial state of the fuel. The timing of a multicycle device would consequently be affected. More generally, our results suggest that smaller initial droplet sizes and some prevaporization or preheating of the fuel expedite detonation transition and, thus, result in efficient performance of liquid-fueled PDEs. For JP-10–air operation, smaller droplets sizes and/or higher levels of prevaporization are required for full performance as compared to JP-10–O_2 mixtures. Finally, our results suggest that in terms of overall propulsive performance, liquid fuels can provide comparable performance to gaseous fuels and should, therefore, be considered a viable option for use in future pulse detonation applications.

Acknowledgments

This work is sponsored by the Office of Naval Research through the Mechanics and Energy Conversion Division's Pulse Detonation Engine Program and the U.S. Naval Research Laboratory 6.1 Computational Physics Task Area. Part of the computer time used in this study was provided by the Department of Defense High Performance Computing Center at the Naval Research Laboratory.

References

[1]Kailasanath, K., "On the Performance of Pulse Detonation Engines," *Confined Detonation and Pulse Detonation Engines*, Torus Press, Moscow, 2003, pp. 191–202.

[2]Webber, W. F., "Spray Combustion in the Presence of a Traveling Wave," *Proceedings of the Combustion Institute*, Vol. 8, Williams and Wilkins, Baltimore, MD, 1962, pp. 1129–1140.

[3]Cramer, F. B., "The Onset of Detonation in a Droplet Combustion Field," *Proceedings of the Combustion Institute*, Vol. 9, Academic Press, New York, 1963, pp. 482–484.

[4]Williams, F. A., "Structure of Detonations in Dilute Sprays," *Physics of Fluids*, Vol. 4, No. 11, 1961, pp. 1434–1443.

[5]Dabora, E. K., Ragland, K. W., and Nicholls, J. A., "Drop Size Effects in Spray Detonations," *Proceedings of the Combustion Institute*, Vol. 12, Combustion Inst., Pittsburgh, PA, 1969, pp. 19–26.

[6]Bowen, J. R., Ragland, K. W., Steffes, F. J., and Loflin, T. G., "Heterogeneous Detonation Supported by Fuel Fogs or Films," *Proceedings of the Combustion Institute*, Vol. 13, Combustion Inst., Pittsburgh, PA, 1971, pp. 1131–1139.

[7]Borisov, A. A., Gelfand, B. E., Gubin, S. A., Kogarko, S. M., and Podgrebenkov, A. L., "The Reaction Zone of Two-Phase Detonations," *Astronautica Acta*, Vol. 15, No. 5, 1970, pp. 411–417.

[8]Kauffman, C. W., and Nicholls, J. A., "Shock-Wave Ignition of Liquid Fuel Drops," *AIAA Journal*, Vol. 9, No. 5, 1971, pp. 880–885.

[9]Bull, D. C., McLeod, M. A., and Mizner, G. A.,"Detonation of Unconfined Fuel Aerosols," *Gasdynamics of Detonations and Explosions*, edited by J. R. Bowen, N. Manson, A. K. Oppenheim, and R. I. Soloukhin, Vol. 75, Progress in Astronautics and Aeronautics, AIAA, New York, 1981, pp. 48–60.

[10]Benedick, W. B., Tieszen, S. R., Knystautas, R., and Lee, J. H. S., "Detonation of Unconfined Large-Scale Fuel Spray-Air Clouds," *Dynamics of Detonations and Explosions: Detonations*, edited by A. L. Kuhl, J. C. Leyer, A. A. Borisov, and W. A. Sirignano, Vol. 133, Progress in Astronautics and Aeronautics, AIAA, Washington, DC, 1991, pp. 297–310.

[11]Brophy, C. M., Netzer, D. W., Sinibaldi, J., and Johnson, R., "Detonation of a JP-10 Aerosol for Pulse Detonation Applications," *High-Speed Deflagration and Detonation: Fundamentals and Control*, ELEX-KM, Moscow, 2001, pp. 207–222.

[12]Bar-Or, R., Sichel, M., and Nicholls, J. A., "The Propagation of Cylindrical Detonations in Monodisperse Sprays," *Proceedings of the Combustion Institute*, Vol. 18, Combustion Inst., Pittsburgh, PA, 1981, pp. 1599–1606.

[13]Papavassiliou, J., Makris, A., Knystautas, R., Lee, J. H. S., Westbrook, C. K., and Pitz, W. J., "Measurements of Cellular Structure in Spray Detonation," *Dynamic Aspects of Explosion Phenomena*, edited by A. L. Kuhl, J. C. Leyer, A. A. Borisov, and W. A. Sirignano, Vol. 154, Progress in Aeronautics and Astronautics, AIAA, Washington, DC, 1993, pp. 148–169.

[14]Ma, F., Wu, Y., Choi, J. Y., and Yang, V., "Thrust Chamber Dynamics of Multi-Tube Pulse Detonation Engines," AIAA Paper 2003-1168, Jan. 2003.

[15]Cambier, J.-L., and Tegner, J. K., "Strategies for Pulsed Detonation Engine Performance Optimization," *Journal of Propulsion and Power*, Vol. 14, No. 4, 1998, pp. 489–498.

[16]Cooper, M., and Shepherd, J. E., "The Effect of Nozzles and Extensions on Detonation Tube Performance," AIAA Paper 2002-3628, July 2002.

[17]Kasahara, J., Arai, T., and Matsuo, A., "Experimental Analysis of Pulse Detonation Engine Performance by Pressure and Momentum Measurements," AIAA Paper 2003-0893, Jan. 2003.

[18]He, X., and Karagozian, A. R., "Numerical Simulation of Pulse Detonation Engine Phenomena," AIAA Paper 2003-1171, Jan. 2003.

[19]Kailasanath, K., Patnaik, G., and Li, C., "The Flowfield and Performance of Pulse Detonation Engines," *Proceedings of the Combustion Institute*, Vol. 29, Combustion Inst., Pittsburgh, PA, 2002, pp. 2855–2862.

[20]Povinelli, L. A., and Yungster, S., "Real Gas Effects on the Performance of Hydrocarbon-Fueled Pulse Detonation Engines," AIAA Paper 2003-0712, Jan. 2003.

[21]Schauer, F., Stutrud, J., and Bradley, R., "Detonation Initiation Studies and Performance Results for Pulsed Detonation Engine Applications," AIAA Paper 2001-1129, Jan. 2001.

[22]Wintenberger, E., Austin, J. M., Cooper, M., Jackson, S., and Shepherd, J. E., "Analytical Model for the Impulse of Single-Cycle Pulse Detonation Tube," *Journal of Propulsion and Power*, Vol. 19, No. 1, 2003, pp. 22–38.

[23]Zitoun, R., and Desbordes, D., "Propulsive Performances of Pulsed Detonations," *Combustion Science and Technology*, Vol. 144, No. 1, 1999, pp. 93–114.

[24]Kailasanath, K., "Recent Developments in the Research on Pulse Detonation Engines," *AIAA Journal*, Vol. 41, No. 2, 2003, pp. 145–159.

[25]Kailasanath, K., "A Review of PDE Research—Performance Estimates," AIAA Paper 2001-0474, Jan. 2001.

[26]Knappe, B. M., and Edwards, C. F., "Results of Decane/Propane Split-Fueled Spray Detonation Experiments," *Proceedings of the Sixteenth ONR Propulsion Meeting*, Office of Naval Research, Arlington, VA, 2003, pp. 117–122.

[27]Fan, W., Yan, C., Huang, X., Zhang, Q., and Zheng, L., "Experimental Investigation on Two-Phase Pulse Detonation Engine," *Combustion and Flame*, Vol. 133, No. 4, 2003, pp. 441–450.

[28]Boris, J. P., and Book, D. L., "Flux-Corrected Transport. 1. SHASTA, A Fluid Transport Algorithm That Works," *Journal of Computational Physics*, Vol. 11, No. 4, 1973, pp. 38–69.

[29]Kailasanath, K., Oran, E. S., Boris, J. P., and Young, T. R., "Determination of Detonation Cell-Size and the Role of Transverse-Waves in Two-Dimensional Detonations," *Combustion and Flame*, Vol. 61, No. 3, 1985, pp. 199–209.

[30]Davidson, D. F., Horning, D. C., Herbon, J. T., and Hanson, R. K., "Shock Tube Measurements of JP-10 Ignition," *Proceedings of the Combustion Institute*, Vol. 28, Combustion Inst., Pittsburgh, PA, 2000, pp. 1687–1692.

[31]Gordon, S., and McBride, B. J., "Computer Program for Calculation of Complex Chemical Equilibrium Compositions, Rocket Performance, Incident and Reflected Shocks, and Chapman–Jouget Detonations," NASA SP-273, NASA Lewis Research Center, Cleveland, OH, 1976.

[32]Igra, O., and Takayama, K., "Shock Tube Study of the Drag Coefficient of a Sphere in a Non-Stationary Flow," *Proceedings of the Royal Society London, Series A: Mathematical and Physical Sciences*, Vol. 442, Aug. 1993, pp. 231–247.

[33]Schiller, L., and Naumann, A. Z., "Uber die Grundlegenden Berechnungen bei der Schwerkraftaufbereitung," *Vereines Deutscher Ingenieure*, Vol. 77, 1933, pp. 318–320.

[34]Faeth, G. M., and Lazar, R. S., "Fuel Droplet Burning Rates in a Combustion Gas Environment," *AIAA Journal*, Vol. 2, No. 11, 1971, pp. 2165–2171.

[35]Sirignano, W. A., *Fluid Dynamics and Transport of Droplets and Sprays*, Cambridge Univ. Press, Cambridge, England, U.K., 1999.

[36]Cheatham, S., and Kailasanath, K., "Numerical Modeling of Liquid-Fueled Detonation in Tubes," *Combustion Theory and Modelling* (to be published).

[37]Kailasanath, K., and Patnaik, G., "Performance Estimates of Pulsed Detonation Engines," *Proceedings of the Combustion Institute*, Vol. 28, Combustion Inst., Pittsburgh, PA, 2000, pp. 595–601.

[38]Harris, P. G., Farinaccio, R., Stowe, R. A., Higgins, A. J., Thibault, P. A., and Laviolette, J. P., "The Effect of DDT Distance on Impulse in a Detonation Tube," AIAA Paper 2001-3467, July 2001.

H. Chelliah
Associate Editor